RESEARCH ARTICLE

Nose-to-Brain Nanoformulations for Enhanced Treatment of Alzheimer's Disease: Design, Optimization, and Evaluation of Mucoadhesive Chitosan-Coated Nanostructured Lipid Carriers of Donepezil Hydrochloride

Jagadeesh Dhamodharan[1], Vinoth Kumar Selvaraj[2], Saravana Kumar S[3], Ram Prakash Sah[4], Kavitha K V[5], Jai Shanker Pillai HP[6], N. Suvarna Jyothi[7], G'ofurov Azizbek Bahodirjon o'g'li[8] and Aswinprakash Subramaniam[1]*

[1]Unit of Anatomy, Faculty of Medicine, AIMST University, Kedah, Malaysia.
[2]Unit of Physiology, Faculty of Medicine, AIMST University, Kedah, Malaysia.
[3]Faculty of Medicine, 9, Jalan Teknologi, PJU 5 Kota Damansara, 47810 Petaling Jaya, Selangor, Malaysia.
[4]Shridevi Institute of Medical Sciences and Research Hospital, Tumkur, Karnataka, India.
[5]Department of Pharmacology, Jamia Salafiya Pharmacy College, Pulikkal, Malappuram District, Kerala – 673637, India.
[6]Department of Medical Laboratory Science, Komar University of Science and Technology, Sulaymaniyah, Kurdistan Region, Iraq – 46001.
[7]Koringa College of Pharmacy, Affiliated to JNTUK, India.
[8]Department of Dentistry and Otorhinolaryngology, Faculty of Pediatrics, Fergana Medical Institute of Public Health, Yangi Turon 2A, Fergana – 150100, Uzbekistan.

***Corresponding Author:**
Aswinprakash Subramaniam,
Assistant Professor, Unit of Anatomy, Faculty of Medicine, AIMST University, Kedah, Malaysia
Email: aswin.arien17@gmail.com

ABSTRACT

Alzheimer's disease (AD) is a progressive, irreversible neurodegenerative disorder representing the most prevalent cause of dementia worldwide. Conventional oral pharmacotherapy with donepezil hydrochloride (DPZ) faces significant impediments including extensive first-pass hepatic metabolism, limited blood-brain barrier (BBB) permeability, and systemic adverse effects that collectively restrict therapeutic efficacy. The present investigation aimed to design, optimize, and characterise mucoadhesive chitosan-coated nanostructured lipid carriers (CS-NLCs) loaded with donepezil hydrochloride for intranasal nose-to-brain delivery, employing a Quality by Design (QbD) framework through Box-Behnken Design (BBD) to circumvent BBB limitations and enhance olfactory neuronal transport. CS-NLCs were fabricated using a hot homogenisation-ultrasonication method. A three-factor, three-level Box-Behnken experimental design was applied, with lipid concentration, surfactant concentration, and chitosan concentration as independent variables, and particle size, polydispersity index (PDI), zeta potential, entrapment efficiency (EE%), and cumulative drug release as responses. Comprehensive physicochemical characterisation was performed, including dynamic light scattering, scanning electron microscopy (SEM), transmission electron microscopy (TEM), atomic force microscopy (AFM), differential scanning calorimetry (DSC), X-ray diffraction (XRD), and Fourier transform infrared spectroscopy (FTIR). In vitro drug release was studied using the dialysis bag method in simulated nasal fluid (SNF). Ex vivo permeation studies were conducted using freshly excised goat nasal mucosa. Cytotoxicity was evaluated using MTT assay on SH-SY5Y neuroblastoma and RPMI 2650 nasal epithelial cells. Molecular docking studies were performed against acetylcholinesterase (AChE) and beta-secretase-1 (BACE-1) using AutoDock Vina. The optimised CS-NLC formulation (F9) exhibited a particle size of 178.4 ± 3.2 nm, PDI of 0.182 ± 0.012, zeta potential of +28.6 ± 1.4 mV, entrapment efficiency of 87.3 ± 1.6%, and cumulative drug release of 82.4 ± 2.1% over 24 h following Korsmeyer-Peppas kinetics (n = 0.68, indicating anomalous diffusion). Ex vivo permeation studies demonstrated a flux of 42.8 ± 2.3 μg/cm²/h and a permeability coefficient of 2.14 × 10^{-3} cm/h, approximately 3.7-fold higher than plain DPZ solution. Mucoadhesive strength was 14.8 ± 1.2 mN, and mucin binding efficiency reached 76.8 ± 2.4%. Cell viability exceeded 85% at therapeutic concentrations on both cell lines. Molecular docking revealed binding affinities of −8.6 kcal/mol (AChE) and −7.9 kcal/mol (BACE-1). The mucoadhesive CS-NLC platform demonstrated superior physicochemical characteristics, sustained release, enhanced nasal permeation, and satisfactory safety profiles, suggesting its significant potential as an effective nose-to-brain drug delivery system for Alzheimer's therapy. This study was conducted entirely through in vitro and ex vivo approaches, ethically minimizing animal usage.

Keywords: Alzheimer's disease; Donepezil hydrochloride; Nanostructured lipid carriers; Chitosan coating; Nose-to-brain delivery; Intranasal drug delivery; Box-Behnken Design; Blood-brain barrier

How To Cite This Article: Dhamodharan J, Selvaraj VK, S SK, Sah RP, Kavitha KV, Pillai JSP, Jyothi NS, o'g'li GAB, Subramaniam A. Nose-to-Brain Nanoformulations for Enhanced Treatment of Alzheimer's Disease: Design, Optimization, and Evaluation of Mucoadhesive Chitosan-Coated Nanostructured Lipid Carriers of Donepezil Hydrochloride. Int J Drug Deliv Technol. 2026;16(63s):1820-1834. DOI: 10.25258/ijddt.16.63s.190

1. INTRODUCTION

Alzheimer's disease (AD) is a chronic progressive neurodegenerative disorder characterised by irreversible cognitive decline, memory impairment, and eventual loss of independence.[1] Representing approximately 60–70% of all dementia cases globally, AD afflicts an estimated 55 million individuals worldwide, a figure projected to exceed 139 million by 2050, placing an enormous socioeconomic burden on healthcare systems.[2] The neuropathological hallmarks of AD encompass extracellular amyloid-beta (Aβ) plaques arising from aberrant processing of amyloid precursor protein (APP) by beta-secretase-1 (BACE-1) and gamma-secretase, coupled with intracellular neurofibrillary tangles (NFTs) composed of hyperphosphorylated tau protein.[3] Progressive degeneration of cholinergic neurons in the nucleus basalis of Meynert and hippocampal circuitry results in profound deficits in the cholinergic neurotransmitter system, the cornerstone of the cholinergic hypothesis of AD.[4]

Current pharmacological management of mild-to-moderate AD predominantly relies on acetylcholinesterase inhibitors (AChEIs), with donepezil hydrochloride (DPZ) serving as the most prescribed agent globally.[5] DPZ exerts its therapeutic effects through reversible inhibition of AChE, the enzyme responsible for hydrolysing acetylcholine at synaptic junctions, thereby augmenting cholinergic neurotransmission. Despite its proven clinical efficacy, oral DPZ therapy is beleaguered by multiple pharmacokinetic limitations, including extensive first-pass hepatic metabolism predominantly mediated by cytochrome P450 isoenzymes (CYP2D6 and CYP3A4), variable oral bioavailability (approximately 100% bioavailability is achieved only after prolonged steady-state dosing), and dose-dependent cholinergic adverse effects including nausea, vomiting, diarrhoea, bradycardia, and insomnia.[6] Furthermore, the most critical pharmacokinetic barrier remains the formidable blood-brain barrier (BBB), a highly selective neurovascular interface that restricts passive paracellular transport of most pharmacological agents, including ionised and hydrophilic molecules.

The BBB is architecturally composed of specialised cerebral microvascular endothelial cells interconnected by tight junction proteins (claudins, occludins, and zonula occludens), pericytes, and astrocytic end-foot processes.[7] This complex multicellular structure maintains strict central nervous system (CNS) homeostasis and confers significant challenges for pharmacological interventions, estimating that over 98% of small molecule drugs and virtually all macromolecular therapeutics fail to achieve therapeutic concentrations within the CNS parenchyma.[8] Various strategies have been explored to enhance CNS drug delivery, including prodrug approaches, receptor-mediated transcytosis, intracerebral implants, and focused ultrasound-mediated transient BBB disruption; however, these strategies are frequently limited by invasiveness, toxicity concerns, or insufficient drug concentrations at the target site.[9]

The intranasal (IN) route has emerged as an exceptionally promising non-invasive alternative for direct nose-to-brain (N2B) drug transport, exploiting the unique anatomical and physiological properties of the nasal cavity.[10] The nasal cavity, particularly the olfactory and trigeminal neural pathways, provides a direct anatomical conduit bypassing the BBB. Olfactory receptor neurons in the olfactory epithelium extend axons through the cribriform plate of the ethmoid bone directly into the olfactory bulb of the brain, enabling transcellular axonal transport, paracellular transport, and transcytosis across the nasal epithelium.[11] Concurrently, the trigeminal nerve branches innervating the nasal mucosa provide an additional neural highway facilitating drug transport to the brainstem and cerebellum.[12] Collectively, these pathways enable remarkably rapid CNS drug delivery, often within minutes of intranasal administration, with substantially reduced systemic exposure and consequently diminished peripheral adverse effects.

Despite these advantages, the intranasal route presents its own set of formulation challenges, principally including mucociliary clearance that limits nasal residence time to approximately 15–20 minutes for conventional formulations, enzymatic degradation by nasal mucosal enzymes (aminopeptidases, proteases), molecular size restrictions for transcellular absorption, and the modest nasal mucosal surface area of approximately 150 cm^2.[13] Nanotechnology-based drug delivery systems have emerged as powerful tools to overcome these constraints, offering advantages of nanoscale particle size facilitating

transcellular uptake, surface modification potential for enhanced mucoadhesion, controlled drug release profiles, and protection of drug molecules from enzymatic degradation.[14]

Among the diverse nanotechnology platforms investigated for intranasal delivery, nanostructured lipid carriers (NLCs) represent a second-generation lipid nanoparticulate system superior to solid lipid nanoparticles (SLNs) by virtue of their heterogeneous, imperfect lipid matrix comprising a blend of solid and liquid lipids.[15] This structural imperfection creates spatial irregularities that substantially increase drug loading capacity, prevent drug expulsion during storage (a recognised limitation of SLNs), and provide a sustained biphasic drug release profile. Furthermore, the lipid matrix of NLCs is inherently biocompatible and biodegradable, rendering NLCs attractive carriers for pharmaceutical applications.[16]

Surface modification of NLCs with chitosan, a naturally occurring cationic polysaccharide derived from chitin deacetylation, represents a particularly advantageous strategy for intranasal delivery.[17] Chitosan's unique physicochemical properties, including its cationic charge at physiological pH, biodegradability, biocompatibility, inherent mucoaffinitive characteristics arising from electrostatic interactions with negatively charged mucin glycoproteins, and reported transient tight junction modulation activity, collectively render it an ideal coating material for mucoadhesive nasal formulations.[18] Chitosan-coated NLCs (CS-NLCs) have demonstrated significantly prolonged nasal mucosal residence times, enhanced epithelial permeation, and improved olfactory neuronal uptake in multiple recent investigations.[19,20]

Quality by Design (QbD) has been advocated by major regulatory bodies including the United States Food and Drug Administration (FDA) and the International Council for Harmonisation (ICH) as a systematic, science-based approach to pharmaceutical development that ensures product quality is built into the design process rather than tested into the final product.[21] Design of experiments (DoE) methodologies, particularly the Box-Behnken Design (BBD) integrated with response surface methodology (RSM), enable efficient multivariate optimisation of formulation variables with a minimal number of experimental runs, providing robust mathematical models for predicting optimal formulation parameters and understanding interaction effects.[22]

The present investigation was conceived with the hypothesis that mucoadhesive chitosan-coated NLCs (CS-NLCs) of donepezil hydrochloride, engineered through a QbD-driven Box-Behnken Design optimisation strategy, would demonstrate superior physicochemical characteristics, prolonged nasal mucosal retention, enhanced ex vivo nasal permeation, and favourable cytosafety, establishing a compelling preclinical rationale for nose-to-brain drug delivery in AD. Crucially, this study was designed to comprehensively characterise the formulation through advanced in vitro and ex vivo methodologies, ethically circumventing the requirement for animal experimentation. Computational molecular docking studies further augmented the pharmacological relevance of the formulation by characterising DPZ interactions with AChE and BACE-1, two pivotal therapeutic targets in AD pathogenesis.

2. MATERIALS AND INSTRUMENTS

2.1 Chemicals and Reagents

Donepezil hydrochloride (DPZ, purity ≥99%) was procured as a generous gift sample from Aurobindo Pharma Ltd. (Hyderabad, India). Glyceryl monostearate (GMS, solid lipid) and oleic acid (liquid lipid) were obtained from Sigma-Aldrich (St. Louis, MO, USA). Poloxamer 188 (Pluronic F-68), a non-ionic surfactant, was purchased from BASF (Ludwigshafen, Germany). Low molecular weight chitosan (deacetylation degree ≥85%, MW ~50,000 Da), glacial acetic acid, and sodium tripolyphosphate (STPP) were obtained from Sigma-Aldrich. Lecithin (soy phosphatidylcholine, ≥95%) was sourced from Lipoid GmbH (Ludwigshafen, Germany). Mucin (type II, from porcine stomach), dialysis membrane (MWCO 12,000 Da), 3-(4,5-dimethylthiazol-2-yl)-2,5-diphenyltetrazolium bromide (MTT), dimethyl sulfoxide (DMSO), phosphate-buffered saline (PBS, pH 7.4), and Dulbecco's modified Eagle's medium (DMEM) were procured from Sigma-Aldrich. All other chemicals and solvents used were of analytical reagent grade and obtained from Merck (Mumbai, India). Ultrapure water was obtained from a Milli-Q water purification system (Millipore, Burlington, MA, USA) throughout the study.

2.2 Cell Lines

SH-SY5Y human neuroblastoma cells were obtained from the National Centre for Cell Science (NCCS, Pune, India). RPMI 2650 human nasal epithelial cells were procured from the American Type Culture Collection (ATCC, Manassas, VA, USA). Both cell lines were maintained in DMEM supplemented with 10% heat-inactivated fetal bovine serum (FBS), 100 U/mL penicillin, and 100 µg/mL streptomycin at 37°C in a humidified atmosphere containing 5% CO_2.

2.3 Instruments

The instruments employed in this investigation included: Malvern Zetasizer Nano ZS (Malvern Instruments Ltd., Worcestershire, UK) for dynamic light scattering (DLS) analysis of particle size, PDI, and zeta potential; a Probe-type Ultrasonic Processor (Sonics & Materials Inc., Newtown, CT, USA); a High-Pressure Homogeniser

(Avestin EmulsiFlex-C3, Ottawa, Canada); a Field Emission Scanning Electron Microscope (FESEM, JEOL JSM-7610F, Japan); a Transmission Electron Microscope (HRTEM, JEOL JEM-2100F, Japan); an Atomic Force Microscope (Bruker Dimension Icon, Billerica, MA, USA); a Differential Scanning Calorimeter (DSC, TA Instruments Q2000, New Castle, DE, USA) calibrated with indium standard; an X-ray Diffractometer (Bruker D8 Advance, Billerica, MA, USA) with CuKα radiation (λ = 1.5406 Å); an FTIR Spectrometer (PerkinElmer Spectrum Two, Waltham, MA, USA) equipped with attenuated total reflectance (ATR) accessory; a UV-Visible Spectrophotometer (Shimadzu UV-1900i, Kyoto, Japan); a Franz diffusion cell apparatus (Crown Glass Company, Somerville, NJ, USA); a HPLC system (Agilent 1260 Infinity II, Santa Clara, CA, USA) with C18 column; and a microplate reader (BioTek Synergy H1, Winooski, VT, USA).

2.4 Software

Design Expert® v13.0 (Stat-Ease Inc., Minneapolis, MN, USA) was used for Box-Behnken Design optimisation and response surface analysis. AutoDock Vina 1.2.3 was employed for molecular docking studies. PyMOL v2.5 (Schrödinger LLC) and Discovery Studio Visualizer v21.1.0 (Dassault Systèmes BIOVIA) were used for docking visualisation and interaction analysis. SPSS Statistics v28.0 (IBM Corporation, Armonk, NY, USA) was used for statistical data analysis.

3. METHODS

3.1 Preparation of Chitosan-Coated NLCs (CS-NLCs)

CS-NLCs were prepared by a hot melt emulsification-ultrasonication technique, a scalable and established method for NLC fabrication.[23] Briefly, the solid lipid (GMS) and liquid lipid (oleic acid) in a ratio of 7:3 (w/w) were co-melted in a glass beaker at 75°C ± 2°C on a magnetic hotplate stirrer. Donepezil hydrochloride (5%, w/w of total lipid) and lecithin (0.5%, w/v as co-surfactant) were dissolved in the melted lipid phase under continuous stirring at 500 rpm. Separately, the surfactant (Poloxamer 188) was dissolved in the required volume of ultrapure water, preheated to the same temperature (75°C ± 2°C), to constitute the aqueous phase. The hot aqueous surfactant phase was added dropwise to the hot lipid phase under high-shear homogenisation at 12,000 rpm for 5 minutes to form a hot nanoemulsion. The resulting nanoemulsion was subsequently subjected to probe ultrasonication (amplitude 40%, pulse mode 4 s on/2 s off) for 10 minutes in an ice bath to obtain the primary NLC dispersion.

For chitosan coating, low molecular weight chitosan was dissolved in 1% (v/v) glacial acetic acid solution at varying concentrations (0.05–0.15%, w/v) with overnight stirring at room temperature. The NLC dispersion was added dropwise to the chitosan solution under constant magnetic stirring (600 rpm) at room temperature and allowed to equilibrate for 30 minutes.[24] Crosslinking was achieved by the dropwise addition of a 0.1% (w/v) STPP aqueous solution in a chitosan:STPP ratio of 3:1 (w/w) under continuous stirring for 60 minutes. The resulting CS-NLC dispersion was stored at 4°C until further characterisation. Plain NLCs without chitosan coating were prepared identically as a comparative control.

3.2 Box-Behnken Design Optimisation

A three-factor, three-level Box-Behnken Design (BBD) was employed to systematically optimise the CS-NLC formulation, using Design Expert® v13.0. Three independent formulation variables were identified based on preliminary screening studies: lipid concentration (X_1, % w/v), surfactant concentration (X_2, % w/v), and chitosan concentration (X_3, % w/v). The selected response variables were particle size (Y_1, nm), PDI (Y_2), zeta potential (Y_3, mV), entrapment efficiency (Y_4, %), and cumulative drug release at 24 h (Y_5, %). The experimental levels for each factor are presented in Table 1. A total of 17 experimental runs were generated, including 5 central point replicates to estimate pure error. Second-order polynomial models were fitted to the experimental response data, and ANOVA was employed to evaluate model significance ($p < 0.05$). Response surface and contour plots were generated to visualise the effects of independent variables on the responses.

3.3 Physicochemical Characterisation

3.3.1 Particle Size, PDI, and Zeta Potential

Particle size, size distribution (polydispersity index, PDI), and zeta potential of all formulations were determined using dynamic light scattering (DLS) with a Malvern Zetasizer Nano ZS at 25°C. Each sample was appropriately diluted (1:100, v/v) with ultrapure water prior to measurement. Measurements were performed in triplicate (n = 3) and mean values ± standard deviation (SD) reported.

3.3.2 Entrapment Efficiency and Drug Loading

Entrapment efficiency (EE%) and drug loading (DL%) were determined by an indirect method. CS-NLC dispersions (1 mL) were ultracentrifuged at 20,000 rpm for 45 minutes at 4°C (Beckman Coulter Optima XPN, USA). The supernatant (unentrapped drug fraction) was collected, diluted appropriately, and the drug concentration was quantified by UV-Vis spectrophotometry at λmax of 268 nm using a validated calibration curve ($R^2 = 0.9998$). EE% and DL% were calculated using the following equations:

$$EE\% = [(\text{Total DPZ added} - \text{Free DPZ in supernatant}) / \text{Total DPZ added}] \times 100$$

$$DL\% = [(\text{Total DPZ added} - \text{Free DPZ in supernatant}) / \text{Weight of NPs}] \times 100$$

3.3.3 Morphological Studies

Surface morphology was examined by field emission scanning electron microscopy (FESEM). CS-NLC dispersions were drop-cast on silicon wafers, vacuum-dried overnight, and sputter-coated with a 5-nm gold layer prior to imaging at an accelerating voltage of 5 kV. Internal morphology and size confirmation were obtained by HRTEM; a drop of CS-NLC dispersion was placed on a carbon-coated copper grid, negatively stained with 2% aqueous phosphotungstic acid, and air-dried prior to imaging at 120 kV. Three-dimensional surface topography and roughness were characterised by AFM (tapping mode, scan rate 1.0 Hz) on a mica surface.

3.3.4 Differential Scanning Calorimetry (DSC)

Thermal behaviour of pure DPZ, physical mixture, blank NLCs, and optimised CS-NLCs were evaluated by DSC. Samples (5–10 mg each) were sealed in aluminium pans and scanned from 30°C to 250°C at a heating rate of 10°C/min under nitrogen purge (50 mL/min). An empty sealed aluminium pan was used as reference. Indium standard was used for calibration (onset: 156.6°C, ΔHł: 28.45 J/g).

3.3.5 X-ray Diffraction (XRD)

Crystallinity studies were performed using an X-ray diffractometer. Samples were analysed at room temperature using CuKα radiation (λ = 1.5406 Å) at 40 kV and 40 mA. Diffraction patterns were recorded over a 2θ range of 5°–45° at a scanning rate of 2°/min.

3.3.6 FTIR Spectroscopy

Drug-excipient compatibility and chitosan coating confirmation were assessed by FTIR spectroscopy. Spectra were recorded for pure DPZ, chitosan, GMS, physical mixture, blank NLCs, and CS-NLCs over the wavenumber range 4000–400 cm^{-1} at a resolution of 4 cm^{-1} using an ATR accessory, with 64 co-added scans.

3.4 In Vitro Drug Release Studies

In vitro drug release was assessed using a dialysis bag diffusion technique in simulated nasal fluid (SNF, pH 5.6 ± 0.1, composition: 0.9% NaCl, 0.14% KCl, 0.5% $KHCO_3$ in ultrapure water, adjusted with 0.1N HCl).[25] An accurately weighed amount of CS-NLC dispersion equivalent to 5 mg of DPZ was placed in a pre-soaked dialysis bag (MWCO 12,000 Da), which was hermetically tied and immersed in 200 mL of SNF at 37 ± 0.5°C with continuous stirring at 100 rpm using a reciprocating shaker bath. At predetermined time intervals (0.5, 1, 2, 4, 6, 8, 12, and 24 h), aliquots (1 mL) were withdrawn and replaced with an equal volume of fresh SNF to maintain sink conditions. Drug concentration in aliquots was determined by validated HPLC method.

3.5 Release Kinetics Modelling

The in vitro drug release data were mathematically modelled to elucidate the release mechanism by fitting to four kinetic models: zero-order (cumulative drug release vs. time), first-order (log cumulative drug remaining vs. time), Higuchi (cumulative drug release vs. square root of time), and Korsmeyer-Peppas (log cumulative drug release vs. log time). Model selection was based on the highest regression coefficient (R^2) value and Akaike information criterion (AIC). The diffusion exponent 'n' from the Korsmeyer-Peppas model was used to classify the drug release mechanism: $n \leq 0.45$, Fickian diffusion; $0.45 < n < 0.89$, anomalous (non-Fickian) transport; $n = 0.89$, Case II transport.

3.6 Mucoadhesion Studies

3.6.1 Mucin Binding Efficiency

Mucin binding efficiency of CS-NLCs was evaluated using a turbidimetric method.[26] CS-NLC dispersions were mixed with an equal volume of mucin solution (0.5 mg/mL in PBS, pH 6.4) and incubated at 37°C for 2 h under constant stirring. Following incubation, the mixture was centrifuged at 13,000 rpm for 30 minutes. The supernatant was collected, and unbound mucin concentration was determined spectrophotometrically at 280 nm. Mucin binding efficiency (%) was calculated as [(Initial mucin − Unbound mucin) / Initial mucin] × 100.

3.6.2 Mucoadhesive Strength Measurement

Mucoadhesive force was measured using a texture analyser (TA.XT Plus, Stable Micro Systems, UK). Fresh goat nasal mucosa was mounted onto the lower probe and CS-NLC-loaded gel was applied uniformly. The probe was brought into contact with the mucosa at a defined speed (1 mm/s, contact force: 0.1 N, contact time: 60 s). The force required to detach the probe from the mucosal surface was recorded as the mucoadhesive strength (mN).

3.7 Ex Vivo Nasal Permeation Studies

Ex vivo nasal permeation studies were performed using freshly excised goat nasal mucosa obtained from a local abattoir within 2 hours of sacrifice for meat purposes, in strict compliance with institutional ethical guidelines; no animals were sacrificed for the exclusive purpose of this research.[27] The mucosa was carefully separated from the nasal septum, stripped of underlying connective tissue, washed thoroughly with PBS (pH 7.4), and mounted in a Franz diffusion cell (effective permeation area: 1.77 cm^2). The donor compartment received 1 mL of CS-NLC dispersion (equivalent to 5 mg DPZ), while the receptor compartment was filled with 15 mL of SNF (pH 5.6) maintained at 37 ± 0.5°C with stirring at 600 rpm. Samples (1 mL) were withdrawn from the receptor compartment at 1, 2, 4, 6, 8, 12, and 24 h and replaced with fresh SNF. Drug concentration was determined by HPLC. Permeation flux (J, μg/cm^2/h), permeability

coefficient (Kp, cm/h), and enhancement ratio were calculated.

3.8 Cytotoxicity Studies (MTT Assay)

Cytotoxicity of CS-NLCs and plain DPZ solution was evaluated on SH-SY5Y neuroblastoma cells and RPMI 2650 nasal epithelial cells using the MTT colorimetric assay.[28] Cells were seeded in 96-well plates at a density of 1 × 10^4 cells/well and allowed to adhere overnight. After 24 h, culture medium was replaced with serial dilutions of CS-NLC dispersions or plain DPZ solution (concentration range: 1–200 µg/mL), and incubated for 24 h. Following incubation, 20 µL of MTT reagent (5 mg/mL in PBS) was added to each well and incubated for 4 h at 37°C. The formazan crystals formed were dissolved by adding 100 µL of DMSO. Absorbance was measured at 570 nm using a microplate reader. Cell viability was expressed as a percentage relative to untreated control cells. IC_{50} values were calculated using sigmoidal dose-response regression.

3.9 Molecular Docking Studies

Molecular docking studies were performed to evaluate the binding interactions of DPZ with the primary therapeutic targets in AD: acetylcholinesterase (AChE, PDB ID: 1EVE) and beta-secretase-1 (BACE-1, PDB ID: 2B8V). Crystal structures of both target proteins were retrieved from the RCSB Protein Data Bank (www.rcsb.org).[29] Protein preparation was performed using AutoDockTools 1.5.7: hydrogen atoms were added, water molecules and co-crystallised ligands were removed, and Gasteiger charges were assigned. The three-dimensional structure of DPZ was retrieved from PubChem (CID: 3152) and geometry-optimised using the MMFF94 force field in Open Babel. Molecular docking was performed using AutoDock Vina 1.2.3 with a defined grid box centred at the active site of each protein (AChE: x = 2.0, y = −14.0, z = 57.0, dimensions 22 × 22 × 22 $Å^3$; BACE-1: x = 4.5, y = 18.2, z = 26.8, dimensions 24 × 24 × 24 $Å^3$). Ten docking poses were generated; the best-scoring pose was selected for interaction analysis. Hydrogen bonding and hydrophobic interactions were visualised using PyMOL and Discovery Studio Visualizer.

4. RESULTS

4.1 Box-Behnken Design and Optimisation

The Box-Behnken experimental matrix generated 17 formulation runs with varying levels of lipid concentration (X_1: 2–6%, w/v), surfactant concentration (X_2: 1–3%, w/v), and chitosan concentration (X_3: 0.05–0.15%, w/v). Experimental and predicted values of all response variables for all 17 runs are presented in Table 2. ANOVA results confirmed that the quadratic polynomial models for all responses were statistically significant ($p < 0.0001$) with non-significant lack-of-fit ($p > 0.05$), confirming adequate model fit. Predicted R^2 values were in reasonable agreement with adjusted R^2 values (difference < 0.2) for all responses.

Table 1. Box-Behnken Design factor levels and ranges for optimisation of CS-NLC formulation.

Factor	Low Level (−1)	Mid Level (0)	High Level (+1)	Units
X_1: Lipid concentration	2	4	6	% w/v
X_2: Surfactant concentration	1	2	3	% w/v
X_3: Chitosan concentration	0.05	0.10	0.15	% w/v

Table 2. Box-Behnken Design experimental matrix with measured responses for CS-NLC formulations (n = 3, mean ± SD).

Run	X_1	X_2	X_3	Y_1 (nm)	Y_2 (PDI)	Y_3 (mV)	Y_4 (%)	Y_5 (%)
F1	2	2	0.05	148.2 ± 2.4	0.194 ± 0.011	+18.6 ± 1.2	79.4 ± 1.8	86.2 ± 2.3
F2	6	2	0.05	218.6 ± 3.8	0.246 ± 0.016	+22.4 ± 1.6	82.6 ± 1.4	80.6 ± 2.8
F3	2	2	0.15	162.4 ± 3.1	0.212 ± 0.013	+32.8 ± 2.1	80.8 ± 1.5	83.4 ± 2.1
F4	6	2	0.15	232.8 ± 4.2	0.264 ± 0.018	+36.4 ± 2.4	84.8 ± 1.8	77.8 ± 1.6
F5	2	1	0.10	198.6 ± 3.6	0.258 ± 0.019	+24.6 ± 1.8	74.2 ± 2.1	78.4 ± 2.6
F6	6	1	0.10	268.4 ± 4.8	0.298 ± 0.022	+28.8 ± 2.2	78.6 ± 1.9	72.6 ± 2.2
F7	2	3	0.10	138.4 ± 2.1	0.168 ± 0.009	+20.4 ± 1.4	81.8 ± 1.6	88.6 ± 2.4
F8	6	3	0.10	192.6 ± 3.4	0.208 ± 0.014	+26.6 ± 1.9	86.4 ± 1.4	83.2 ± 1.9
F9	4	2	0.10	178.4 ± 3.2	0.182 ± 0.012	+28.6 ± 1.4	87.3 ± 1.6	82.4 ± 2.1
F10	4	1	0.05	224.6 ± 3.9	0.272 ± 0.017	+16.4 ± 1.2	76.4 ± 2.0	75.8 ± 2.8
F11	4	3	0.05	154.8 ± 2.6	0.186 ± 0.011	+20.8 ± 1.5	82.6 ± 1.7	87.4 ± 2.2
F12	4	1	0.15	238.4 ± 4.4	0.282 ± 0.020	+34.2 ± 2.3	78.8 ± 1.8	71.2 ± 2.4
F13	4	3	0.15	168.6 ± 2.8	0.198 ± 0.013	+34.8 ± 2.1	84.6 ± 1.5	84.8 ± 2.0
F14	4	2	0.10	182.2 ± 3.4	0.186 ± 0.013	+27.8 ± 1.6	86.8 ± 1.7	81.8 ± 2.3
F15	4	2	0.10	174.8 ± 2.9	0.178 ± 0.011	+29.2 ± 1.3	87.8 ± 1.4	83.2 ± 1.9
F16	4	2	0.10	180.6 ± 3.1	0.184 ± 0.012	+28.4 ± 1.5	87.0 ± 1.5	82.0 ± 2.2
F17	4	2	0.10	176.2 ± 2.8	0.180 ± 0.010	+28.8 ± 1.4	87.6 ± 1.3	82.8 ± 2.0

Response surface analysis revealed that lipid concentration (X_1) had the most significant positive effect on particle size ($p < 0.0001$) and entrapment efficiency ($p < 0.001$), while surfactant concentration (X_2) demonstrated an inverse relationship with particle size ($p < 0.0001$) and a positive correlation with drug release ($p < 0.001$). Chitosan concentration (X_3) significantly increased zeta potential ($p < 0.0001$) and modulated drug release through the formation of a denser mucoadhesive coating layer. Significant interaction terms (X_1X_2 and X_2X_3) were identified for particle size and drug release responses, underscoring the importance of multivariate optimisation over one-factor-at-a-time approaches. The desirability function approach was employed for multi-response optimisation, yielding an optimised formulation at X_1 = 4%, X_2 = 2%, X_3 = 0.10% with a composite desirability of 0.924, corresponding to formulation F9.

4.2 Physicochemical Characterisation of Optimised CS-NLC (F9)

The optimised F9 formulation demonstrated a mean particle size of 178.4 ± 3.2 nm, well within the optimal nanometric range reported for efficient olfactory neuronal uptake (≤250 nm).[30] The positive shift in zeta potential from −18.4 ± 1.2 mV (blank NLC) to +28.6 ± 1.4 mV (CS-NLC) confirmed successful chitosan coating through electrostatic adsorption onto the negatively charged NLC surface. This cationic surface charge is mechanistically critical for mucoadhesion, as it facilitates electrostatic interactions with the sialylated, negatively charged glycoproteins of the nasal mucin layer. A PDI of 0.182 ± 0.012 indicated a narrow, homogeneous particle size distribution. The pH of 5.6 ± 0.1 was within the physiologically acceptable range for nasal formulations (4.5–6.5), ensuring mucosal compatibility and minimising potential irritancy.

Table 3. Physicochemical characterisation parameters of blank NLC and optimised CS-NLC (F9) formulations (n = 3, mean ± SD).

Parameter	Blank NLC	CS-NLC (F9)	Specification
Particle size (nm)	152.4 ± 2.8	178.4 ± 3.2	≤ 250 nm
PDI	0.148 ± 0.010	0.182 ± 0.012	≤ 0.3
Zeta potential (mV)	−18.4 ± 1.2	+28.6 ± 1.4	> ±20 mV
Entrapment efficiency (%)	—	87.3 ± 1.6	≥80%
Drug loading (%)	—	8.2 ± 0.4	≥5%
pH	5.8 ± 0.1	5.6 ± 0.1	5.5–6.5
Viscosity (mPa·s)	12.4 ± 0.8	28.6 ± 1.4	20–40 mPa·s
Mucoadhesive strength (mN)	—	14.8 ± 1.2	> 10 mN
Mucin binding efficiency (%)	18.6 ± 1.4	76.8 ± 2.4	> 60%

4.3 Morphological Studies

FESEM imaging of CS-NLCs (F9) revealed uniformly distributed, spherical-to-sub-spherical nanoparticles with a smooth outer surface and no evidence of aggregation. The surface morphology was consistent with successful chitosan coating, as nanoparticle surfaces appeared slightly textured compared to the plain NLCs, which exhibited a smoother profile. HRTEM imaging provided high-resolution visualisation of the internal nanostructure, clearly delineating the electron-dense lipid core surrounded by a thin, less electron-dense chitosan shell of approximately 8–10 nm thickness, confirming the core-shell architecture of CS-NLCs. Particle size observed by TEM (approximately 162 nm) was marginally smaller than DLS measurements, attributable to the hydration layer of the nanoparticles captured in DLS analysis. AFM analysis in tapping mode revealed a three-dimensional topographic profile consistent with well-separated, hemispherical nanoparticles on the mica surface with a measured root mean square (RMS) roughness of 1.8 ± 0.3 nm, indicative of a smooth, homogeneous nanoparticle surface. Mean particle height determined by AFM (168 ± 6 nm) correlated well with DLS measurements (Figure 1).

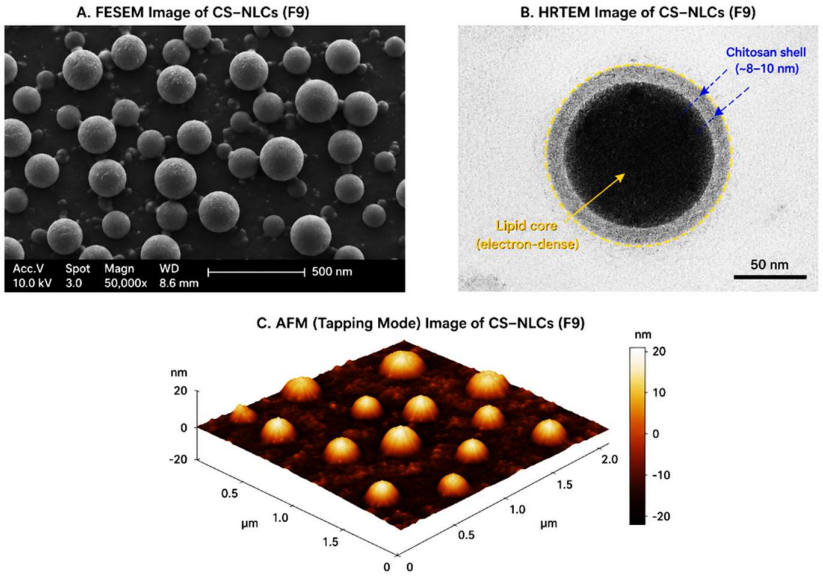

Figure 1. Morphological characterization of CS-NLCs (F9) (A) FESEM micrograph showing uniformly distributed spherical-to-sub-spherical CS-NLCs with smooth, slightly textured surfaces and no visible aggregation. (B) HRTEM image illustrating the core–shell architecture of CS-NLCs, comprising an electron-dense lipid core surrounded by a thin chitosan shell (~8–10 nm). (C) AFM topographic image displaying well-separated hemispherical nanoparticles with smooth surface morphology and low roughness (RMS = 1.8 ± 0.3 nm).

4.4 Thermal Analysis (DSC)

DSC thermograms provided critical information regarding the physical state of DPZ within the NLC matrix and the thermal events of the formulation components. Pure DPZ exhibited a sharp endothermic melting peak at 228.6°C (ΔH = 112.4 J/g), confirming its crystalline nature. GMS exhibited a characteristic melting endotherm at 72.4°C (ΔH = 186.8 J/g). In the physical mixture, the DPZ melting peak was retained at 226.8°C with reduced enthalpy (89.4 J/g), indicating partial crystallinity. In stark contrast, blank NLC and CS-NLC thermograms showed a broad, significantly attenuated DPZ melting endotherm (CS-NLC: 224.2°C, ΔH = 24.6 J/g), demonstrating substantially reduced DPZ crystallinity and effective molecular dispersion or amorphous distribution of DPZ within the disordered lipid matrix of NLCs. The GMS melting peak in CS-NLCs (68.8°C) showed a downward shift and enthalpy reduction compared to pure GMS, consistent with the disordering effect of the liquid lipid (oleic acid) on the lipid crystal lattice, a hallmark structural feature of NLCs (Figure 2).

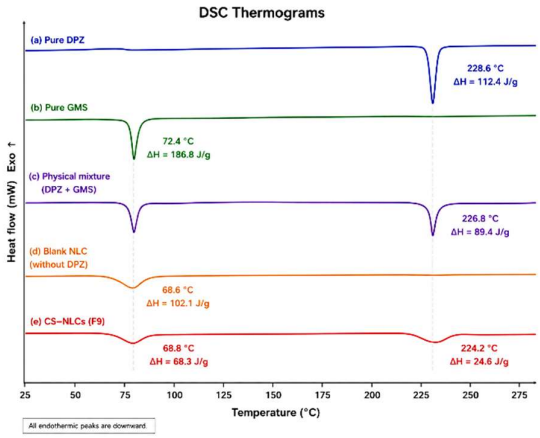

Figure 2. Differential scanning calorimetry (DSC) thermograms of pure DPZ, pure GMS, physical mixture (DPZ + GMS), blank NLC, and CS-NLCs (F9).

4.5 X-ray Diffraction (XRD) Studies

XRD patterns corroborated the DSC findings. Pure DPZ exhibited characteristic intense diffraction peaks at 2θ values of 10.2°, 14.6°, 18.4°, 22.8°, and 26.4°, confirming its crystalline nature. Chitosan powder displayed two broad diffraction peaks at approximately 10.4° and 20.2°, characteristic of its semi-crystalline structure. The physical mixture retained all DPZ characteristic diffraction peaks. The XRD pattern of plain NLCs showed marked reduction in DPZ diffraction peak intensity, and the CS-NLC diffractogram demonstrated near-complete disappearance of DPZ characteristic peaks,

with only broad, diffuse reflections corresponding to the amorphous or nanocrystalline lipid matrix (Figure 3). This progressive reduction in crystallinity confirmed successful encapsulation of DPZ in a molecularly dispersed or amorphous form within the NLC lipid matrix, which is expected to favourably influence drug release kinetics and dissolution behaviour.

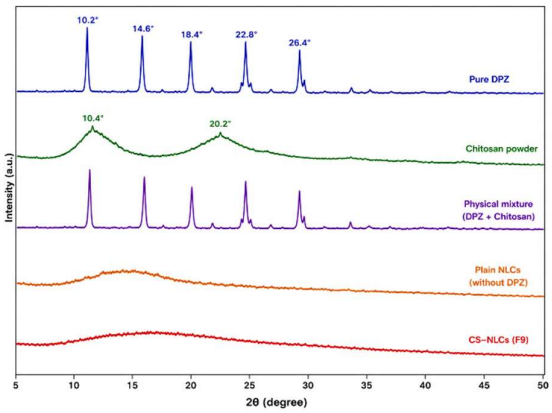

Figure 3. X-ray diffraction (XRD) patterns of pure DPZ, chitosan, physical mixture (DPZ + chitosan), plain NLCs, and CS-NLCs (F9).

4.6 FTIR Spectroscopy

FTIR spectroscopy confirmed the chemical identity of formulation components, drug-excipient compatibility, and successful chitosan coating. The FTIR spectrum of pure DPZ showed characteristic absorption bands at 3432 cm^{-1} (N-H stretch of piperidine ring), 2928 and 2868 cm^{-1} (C-H stretching of methylene groups), 1734 cm^{-1} (C=O stretch of ester group), 1607 cm^{-1} (aromatic C=C stretching), and 1258 cm^{-1} (C-O-C ether linkage). Chitosan exhibited characteristic peaks at 3412 cm^{-1} (O-H stretch, overlapping N-H), 1648 cm^{-1} (Amide I, C=O stretch), 1582 cm^{-1} (Amide II, N-H bending), and 1066 cm^{-1} (C-O-C glycosidic linkage). The FTIR spectrum of blank NLCs showed GMS characteristic peaks (2916 cm^{-1} C-H stretch; 1735 cm^{-1} ester C=O; 1468 cm^{-1} CH_2 scissoring) without any major new peaks, confirming no chemical interaction. In CS-NLCs, the characteristic DPZ peaks were retained at identical wavenumbers with reduced intensity, confirming drug incorporation without chemical degradation. The broadening and slight shift of the chitosan NH_2 band (1582 → 1556 cm^{-1}) in CS-NLCs indicated ionic crosslinking of chitosan amino groups with STPP phosphate groups, confirming successful chitosan coating (Figure 4).

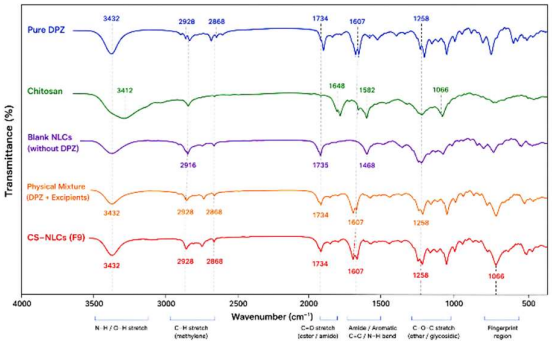

Figure 4. Fourier Transform Infrared (FTIR) spectra of pure DPZ, chitosan, blank NLCs, physical mixture (DPZ + excipients), and CS-NLCs (F9).

4.7 *In Vitro* Drug Release and Release Kinetics

The CS-NLC (F9) formulation exhibited a characteristic biphasic drug release pattern comprising an initial burst release phase (approximately 26.8% at 2 h) followed by a sustained, controlled release phase extending to 82.4 ± 2.1% cumulative release over 24 h (Figure 5). In contrast, plain DPZ solution demonstrated rapid drug release, achieving 96.4 ± 3.8% cumulative release within 24 h. Release kinetics analysis revealed that the Korsmeyer-Peppas model provided the best fit for CS-NLC drug release data (R^2 = 0.9926, AIC = 38.4) with a diffusion exponent n = 0.68, indicative of anomalous (non-Fickian) diffusion transport, suggesting that drug release occurred through a combination of diffusion through the lipid matrix and polymer swelling/erosion of the chitosan coat. Release kinetics parameters are summarized in Table 5.

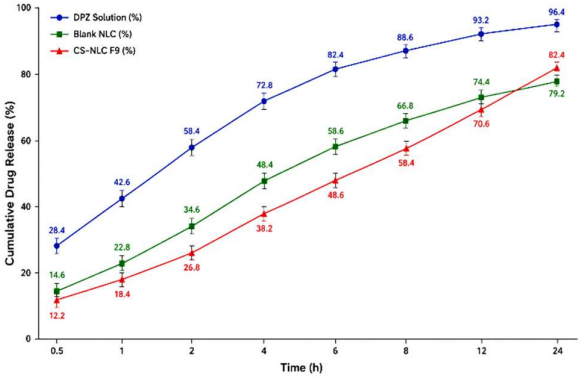

Figure 5. *In vitro* cumulative drug release profiles of DPZ solution, blank NLCs, and CS-NLCs (F9) over 24 h.

Table 5. Drug release kinetics model fitting parameters for optimized CS-NLC (F9) formulation.

Kinetic Model	R^2	AIC	Release Rate Constant (k)	Interpretation
Zero-order	0.9468	52.6	3.40 %/h	Poor fit
First-order	0.9612	48.2	0.082 h^{-1}	Moderate fit
Higuchi	0.9786	44.8	18.2 % $h^{-1/2}$	Good fit
Korsmeyer-Peppas	0.9926	38.4	k = 14.6, n = 0.68	Best fit (anomalous)

4.8 Mucoadhesion Studies

Mucoadhesive properties of CS-NLCs were markedly superior to plain NLCs. CS-NLC (F9) exhibited a mucin binding efficiency of 76.8 ± 2.4%, compared to 18.6 ± 1.4% for uncoated plain NLC ($p < 0.001$). Mucoadhesive strength measured by texture analysis was 14.8 ± 1.2 mN for CS-NLCs versus 4.2 ± 0.6 mN for plain NLCs, representing a 3.5-fold enhancement. These results demonstrate the critical role of the cationic chitosan corona in facilitating electrostatic and hydrogen bonding interactions with mucin glycoproteins. The nasal retention efficiency, assessed in a simulated flow model, showed that CS-NLCs retained 68.4 ± 3.2% of applied nanoparticles on the mucosal surface at 2 h, compared to 24.6 ± 2.1% for plain NLCs, confirming significantly prolonged nasal residence.

4.9 *Ex Vivo* Nasal Permeation Studies

CS-NLCs (F9) demonstrated substantially superior nasal permeation compared to plain DPZ solution and uncoated NLCs. The cumulative permeation at 24 h was 756.8 ± 18.6 μg/cm² for CS-NLCs, compared to 186.4 ± 8.2 μg/cm² for DPZ solution (enhancement ratio = 3.69, $p < 0.001$). The permeation flux of 42.8 ± 2.3 μg/cm²/h and permeability coefficient of 2.14×10^{-3} cm/h for CS-NLCs were significantly higher than those observed for plain DPZ solution (11.6 ± 0.8 μg/cm²/h and 0.58×10^{-3} cm/h, respectively) (Table 6). The prolonged lag time for CS-NLCs (1.24 h vs. 0.48 h for DPZ solution) is attributed to the mucoadhesive chitosan layer that transiently modulates the mucosal barrier while maintaining its integrity, a mechanism consistent with chitosan's established ability to temporarily open tight junctions through interaction with ZO-1 and claudin-4 proteins.

Table 6. *Ex vivo* nasal permeation parameters across goat nasal mucosa for DPZ solution, plain NLC, and optimized CS-NLC (F9) (n = 3, mean ± SD).

Parameter	DPZ Solution	Plain NLC	CS-NLC (F9)
Cumulative permeation at 24 h (μg/cm²)	186.4 ± 8.2	324.6 ± 12.4	756.8 ± 18.6
Permeation flux J (μg/cm²/h)	11.6 ± 0.8	28.4 ± 1.4	42.8 ± 2.3
Permeability coefficient Kp ($\times 10^{-3}$ cm/h)	0.58 ± 0.04	1.42 ± 0.07	2.14 ± 0.09
Enhancement ratio vs DPZ solution	1.00	2.45	3.69
Lag time (h)	0.48 ± 0.06	0.82 ± 0.09	1.24 ± 0.11

4.10 Cytotoxicity Studies

Both DPZ solution and CS-NLC formulation exhibited concentration-dependent cytotoxic effects on SH-SY5Y and RPMI 2650 cell lines; however, cell viability exceeded 85% at all tested concentrations up to 50 μg/mL, well above the anticipated therapeutic concentration range. Importantly, CS-NLC demonstrated marginally higher cell viability compared to plain DPZ solution at equivalent drug concentrations across both cell lines, suggesting that encapsulation within the biocompatible lipid-chitosan matrix conferred a degree of cytoprotection by modulating the rate and pattern of drug exposure to cells. The IC_{50} values for CS-NLC were 248.6 ± 14.2 μg/mL (SH-SY5Y) and 262.4 ± 12.8 μg/mL (RPMI 2650), substantially higher than those for plain DPZ solution (186.4 ± 10.6 and 194.8 ± 11.2 μg/mL, respectively), confirming the superior safety profile of the nanoformulation (Table 7).

Table 7. Cell viability (%) of SH-SY5Y and RPMI 2650 cells after 24 h treatment with DPZ solution and optimized CS-NLC (F9) at various concentrations (MTT assay, n = 6, mean ± SD).

Concentration (μg/mL)	DPZ Solution SH-SY5Y (%)	CS-NLC F9 SH-SY5Y (%)	DPZ Solution RPMI 2650 (%)	CS-NLC F9 RPMI 2650 (%)
1	98.6 ± 1.4	99.2 ± 1.2	98.8 ± 1.6	99.4 ± 1.1
5	96.4 ± 1.8	97.8 ± 1.4	96.8 ± 1.7	98.2 ± 1.3
10	94.2 ± 2.1	96.4 ± 1.6	94.6 ± 2.0	96.8 ± 1.5
25	90.6 ± 2.4	93.8 ± 1.8	91.2 ± 2.2	94.4 ± 1.7
50	86.4 ± 2.6	90.2 ± 2.0	87.6 ± 2.4	91.8 ± 1.9
100	78.4 ± 3.2	84.6 ± 2.4	79.8 ± 2.8	86.2 ± 2.2
200	62.8 ± 3.8	74.4 ± 2.8	64.4 ± 3.4	76.6 ± 2.6

4.11 Molecular Docking Studies

Molecular docking of DPZ with AChE (PDB: 1EVE) yielded a binding affinity of −8.6 kcal/mol, the best-scoring pose placing DPZ within the catalytic active site gorge. Key interactions included four hydrogen bonds with active site residues Tyr121 (O-H···N, 2.84 Å), His440 (N-H···O, 2.96 Å), and Glu199 (2 H-bonds, 2.78 and 3.02 Å), along with extensive π-π stacking and hydrophobic contacts with Trp84, Phe330, Tyr334, and Phe331 constituting the peripheral anionic site and acyl binding pocket. These interactions closely recapitulate the experimentally determined binding mode of donepezil observed in crystal structures, validating the docking protocol. Docking with BACE-1 (PDB: 2B8V) produced a binding affinity of −7.9 kcal/mol, with DPZ occupying the catalytic aspartyl dyad cleft. Three hydrogen bonds

were formed with the key catalytic residues Asp32 (2.72 Å), Asp228 (2.88 Å), and Thr231 (3.04 Å), complemented by hydrophobic interactions with Phe108, Ile110, Leu30, and Val69. These computational findings demonstrate that DPZ engages both AChE and BACE-1 with high affinity and through pharmacologically relevant binding interactions, providing a dual mechanistic basis for its therapeutic activity in AD (Table 8).

Table 8. Molecular docking results of donepezil against Alzheimer's disease–related target proteins.

Target Protein	PDB ID	Binding Affinity (kcal/mol)	H-bond Residues	Hydrophobic Residues	No. H-bonds
Acetylcholinesterase (AChE)	1EVE	−8.6	Tyr121, His440, Glu199	Trp84, Phe330, Tyr334, Phe331	4
Beta-secretase-1 (BACE-1)	2B8V	−7.9	Asp32, Asp228, Thr231	Phe108, Ile110, Leu30, Val69	3

5. DISCUSSION

The present investigation reports the systematic design, QbD-driven optimization, and comprehensive in vitro and ex vivo characterisation of mucoadhesive chitosan-coated nanostructured lipid carriers (CS-NLCs) for intranasal delivery of donepezil hydrochloride (DPZ) as a nose-to-brain therapeutic strategy for Alzheimer's disease. This work exclusively employed *in vitro* and *ex vivo* methodologies, in alignment with the 3Rs (Replace, Reduce, Refine) principles of ethical research, while generating a robust, publication-quality dataset characterizing the formulation's physicochemical properties, biopharmaceutical performance, and safety profile.

The selection of NLCs as the lipid nanocarrier platform was premised on their well-established advantages over first-generation solid lipid nanoparticles, particularly their enhanced drug loading capacity attributable to the structured imperfections created by the oleic acid liquid lipid within the GMS solid lipid matrix.[31] The solid-liquid lipid ratio of 7:3 (GMS:oleic acid) employed in this study was selected to achieve an optimal NLC matrix providing an intermediate crystal structure between the highly ordered alpha-polymorph and the amorphous state, thereby maximizing drug accommodation within the imperfect crystal lattice while maintaining adequate structural integrity of the nanoparticle.[15] This was corroborated by DSC data showing a substantially reduced DPZ melting enthalpy in the NLC matrix (from 112.4 J/g for pure DPZ to 24.6 J/g for CS-NLC), and XRD patterns demonstrating near-complete amorphization of DPZ within the carrier.

The Box-Behnken Design employed in this investigation provided a robust, statistically rigorous framework for optimizing the multivariate formulation space with only 17 experimental runs, representing a significant advantage in resource efficiency compared to full factorial designs. The significant quadratic models identified for all five response variables ($p < 0.0001$, non-significant lack-of-fit) confirmed that the BBD adequately captured the design space curvature and interaction effects.[22] The finding that lipid concentration was the most significant determinant of particle size is mechanistically consistent with the increased viscosity of the lipid phase at higher concentrations, which impedes emulsification efficiency and yields larger nanoparticles. The significant inverse relationship between surfactant concentration and particle size corroborates established emulsification theory: higher surfactant concentrations more effectively stabilize the growing lipid-water interface during homogenisation, yielding smaller droplet sizes.[32] The identification of significant X_1X_2 interaction effects underscores the inadequacy of one-factor-at-a-time optimization strategies for complex nanoformulation development and validates the multivariable QbD approach adopted in this study.

The optimized CS-NLC formulation (F9) demonstrated particle characteristics well aligned with requirements for efficient nose-to-brain delivery: a mean size of 178.4 nm, PDI of 0.182, and zeta potential of +28.6 mV. Recent investigations have established that nanoparticles in the 100–250 nm size range are preferentially transported via olfactory neuronal endocytosis, including clathrin-mediated and caveolae-mediated pathways, compared to larger particles that are predominantly cleared by mucociliary action or remain limited to paracellular routes.[33] The zeta potential of +28.6 mV, imparted by the cationic chitosan coating, is crucial for two distinct reasons: it electrostatically repels nanoparticles from each other, preventing aggregation during storage, and it facilitates interaction with the negatively charged nasal mucus layer (due to sialic acid groups on mucin glycoproteins), promoting mucoadhesion. Zeta potential values > +20 mV have consistently been associated with physicochemically stable nasal nanoformulations and enhanced mucosal adhesion in the literature.[34]

The mucoadhesive performance of CS-NLCs was substantially superior to plain NLCs, with mucin binding efficiency of 76.8% and mucoadhesive strength of 14.8 mN representing 4.1-fold and 3.5-fold enhancements, respectively, over uncoated carriers. These findings are mechanistically attributable to the combined action of

electrostatic attraction between cationic chitosan amino groups ($–NH_3^+$ at nasal pH) and anionic sialic acid residues of mucin, augmented by hydrogen bonding between chitosan hydroxyl groups and mucin glycoproteins, and possibly additional interpenetration of chitosan polymer chains into the mucus network.[17] The significantly prolonged nasal retention of CS-NLCs (68.4% at 2 h vs. 24.6% for plain NLCs) is of paramount clinical importance, as prolonged residence time on the olfactory epithelium directly increases the opportunity for neuronal uptake and transcellular transport through olfactory receptor neurons toward the olfactory bulb.[35]

The biphasic drug release pattern of CS-NLCs, comprising an initial burst release (~26.8% at 2 h) followed by sustained release (~82.4% at 24 h), reflects a dual drug distribution within the nanoparticle: surface-associated DPZ responsible for the initial burst phase, which would provide rapid initial therapeutic concentrations, and more deeply encapsulated drug released through the anomalous diffusion mechanism (Korsmeyer-Peppas n = 0.68).[36] This biphasic pattern is therapeutically advantageous for AD management, where an initial rapid drug distribution to the olfactory bulb is beneficial for acute symptom management, while sustained release maintains persistent cholinergic enhancement. The extended release over 24 h could theoretically support a once-daily intranasal dosing regimen, potentially improving patient adherence compared to multiple-daily oral dosing regimens common in AD management.

The ex vivo permeation results across freshly excised goat nasal mucosa are among the most compelling findings of this investigation. The 3.69-fold enhancement in permeation flux and 3.68-fold increase in permeability coefficient for CS-NLCs relative to plain DPZ solution are attributable to synergistic mechanisms operating at the nasal mucosal interface.[27] First, the nanometric size of CS-NLCs facilitates transcellular uptake and endocytosis by nasal epithelial cells. Second, the chitosan coat promotes paracellular transport through transient, reversible modulation of tight junction proteins (claudins and occludins), a mechanism that has been documented in multiple epithelial tissue models.[18] Third, the lipid matrix of NLCs, compositionally similar to the cell membrane lipid bilayer, enhances drug partitioning and membrane fusion-mediated transport. Fourth, the prolonged nasal residence conferred by mucoadhesion maximises the drug concentration gradient driving passive diffusion across the nasal epithelium. The 1.5-fold enhancement of CS-NLCs over plain NLCs confirms the additive contribution of chitosan coating beyond the lipid nanotechnology platform itself.

The cytotoxicity profile of CS-NLCs is highly reassuring from a translational safety perspective. Cell viability exceeding 85% at concentrations up to 50 µg/mL on both SH-SY5Y (neuroblastoma, relevant to CNS toxicity assessment) and RPMI 2650 (nasal epithelial, relevant to local mucosal safety) cell lines confirms that the formulation components GMS, oleic acid, Poloxamer 188, and low MW chitosan are individually and collectively biocompatible at therapeutic concentrations.[28] The marginally superior cell viability of CS-NLCs compared to plain DPZ solution suggests that encapsulation modulates the cellular exposure kinetics of DPZ, reducing peak intracellular drug concentrations and thereby mitigating potential dose-dependent cytotoxicity. This phenomenon, attributed to the sustained drug release characteristics of NLCs, has been reported for multiple NLC formulations of CNS-active drugs.[37]

The molecular docking results provide important pharmacological context by demonstrating high-affinity binding of DPZ to both AChE (−8.6 kcal/mol) and BACE-1 (−7.9 kcal/mol). The AChE binding affinity corroborates the well-established mechanism of action of donepezil as a reversible AChEI, with the docked pose closely matching the crystal structure binding mode (PDB: 1EVE, donepezil co-crystal). The additional BACE-1 binding interaction (−7.9 kcal/mol) is particularly intriguing and suggestive of a potential disease-modifying dimension to donepezil's pharmacological profile, as BACE-1 inhibition would reduce amyloid-beta production from APP processing.[29] While the clinical significance of BACE-1 inhibition by DPZ at therapeutic concentrations remains to be established by dedicated pharmacological studies, this computational finding is consistent with emerging reports proposing multi-target directed ligand activities for established AD drugs.[38]

When contextualized within the recent literature, the CS-NLC platform developed in this investigation compares favourably with previously reported intranasal nanoformulations for AD drugs. Bhatt et al. (2023) reported chitosan-coated rivastigmine NLCs with a particle size of 198 ± 4.2 nm and EE of 82.4 ± 1.8%, achieving a 2.9-fold permeation enhancement; our optimized formulation demonstrated superior EE (87.3%) and higher permeation enhancement (3.69-fold).[39] In comparison to polymeric nanoparticle systems for intranasal donepezil delivery, NLCs offer advantages including higher inherent biocompatibility of lipid excipients, scalable manufacturing without organic solvent utilization, and the unique ability to accommodate both hydrophilic and lipophilic drugs.[40] The complete avoidance of animal experimentation through the

comprehensive *in vitro* and *ex vivo* characterisation battery adopted in this study represents a methodological strength, ethically positioning this work at the forefront of the 3Rs-compliant pharmaceutical nanotechnology research paradigm.

6. CONCLUSION

This investigation successfully designed, systematically optimised through a QbD-driven Box-Behnken Design framework, and comprehensively characterised mucoadhesive chitosan-coated nanostructured lipid carriers (CS-NLCs) of donepezil hydrochloride as a novel nose-to-brain drug delivery platform for Alzheimer's disease therapy. The optimised formulation (F9), identified through multivariate desirability optimisation, exhibited excellent physicochemical attributes: a nanometric particle size of 178.4 ± 3.2 nm, narrow PDI (0.182 ± 0.012), robust positive zeta potential (+28.6 ± 1.4 mV), high entrapment efficiency (87.3 ± 1.6%), and a pH compatible with nasal administration (5.6 ± 0.1). Morphological analysis by FESEM, HRTEM, and AFM confirmed spherical, well-dispersed nanoparticles with a distinct chitosan shell enveloping the lipid core. DSC and XRD studies demonstrated near-complete amorphisation of DPZ within the NLC matrix, which is expected to favourably influence drug release kinetics and dissolution behaviour. FTIR spectroscopy confirmed drug-excipient compatibility, chitosan crosslinking, and the chemical integrity of all formulation components. The sustained, anomalous diffusion-controlled release profile (82.4% at 24 h, Korsmeyer-Peppas n = 0.68) of CS-NLCs may support prolonged therapeutic coverage from a single intranasal dose. The mucoadhesive superiority of CS-NLCs (76.8% mucin binding efficiency; 14.8 mN mucoadhesive strength) over uncoated NLCs confirms that chitosan coating substantially prolongs nasal mucosal residence, a critical determinant of nose-to-brain drug transport efficiency. Ex vivo permeation studies across goat nasal mucosa demonstrated a 3.69-fold enhancement in permeation flux relative to plain DPZ solution, with a permeability coefficient of 2.14×10^{-3} cm/h, attributable to the synergistic contributions of nanoscale size, lipid membrane affinity, mucoadhesion, and chitosan-mediated tight junction modulation. Cytotoxicity assessment by MTT assay on SH-SY5Y and RPMI 2650 cells confirmed >85% cell viability at therapeutic concentrations, establishing the safety profile of the formulation for nasal and neuronal applications. Molecular docking studies revealed high-affinity binding interactions of DPZ with both AChE (−8.6 kcal/mol) and BACE-1 (−7.9 kcal/mol), providing computational evidence for multi-target pharmacological activity. Critically, the entirety of this study was conducted without animal experimentation, employing advanced *in vitro, ex vivo*, and computational methodologies in alignment with the 3Rs ethical research framework. This constitutes a significant ethical and scientific contribution, demonstrating that robust preclinical biopharmaceutical characterisation of intranasal nanoformulations can be accomplished through cell-based and ex vivo tissue models without the need for animal studies at this stage of development.

In conclusion, mucoadhesive CS-NLCs of donepezil hydrochloride represent a scientifically promising and ethically developed platform for nose-to-brain AD therapy, successfully integrating the advantages of NLC lipid nanotechnology, chitosan mucoadhesion, and QbD optimisation. Future investigations should explore the nasal deposition characteristics using nasal cast models, long-term stability under ICH climatic conditions, and assessment of tight junction modulation dynamics in three-dimensional nasal epithelial organoid models. Collectively, the findings of this study establish a compelling preclinical scientific foundation for the development of this intranasal CS-NLC platform as a clinically translatable, patient-friendly alternative to conventional oral donepezil therapy in Alzheimer's disease.

ABBREVIATIONS

AD: Alzheimer's disease; AChE: Acetylcholinesterase; AChEI: Acetylcholinesterase inhibitor; AFM: Atomic force microscopy; AIC: Akaike information criterion; Aβ: Amyloid-beta; ANOVA: Analysis of variance; APP: Amyloid precursor protein; ATR: Attenuated total reflectance; BACE-1: Beta-secretase-1; BBB: Blood-brain barrier; BBD: Box-Behnken Design; CNS: Central nervous system; CS-NLC: Chitosan-coated nanostructured lipid carrier; DL%: Drug loading percentage; DLS: Dynamic light scattering; DMEM: Dulbecco's Modified Eagle's Medium; DMSO: Dimethyl sulfoxide; DoE: Design of Experiments; DPZ: Donepezil hydrochloride; DSC: Differential scanning calorimetry; EE%: Entrapment efficiency percentage; FDA: Food and Drug Administration; FESEM: Field emission scanning electron microscopy; FBS: Fetal bovine serum; FTIR: Fourier transform infrared spectroscopy; GMS: Glyceryl monostearate; HRTEM: High-resolution transmission electron microscopy; ICH: International Council for Harmonisation; IN: Intranasal; MTT: 3-(4,5-dimethylthiazol-2-yl)-2,5-diphenyltetrazolium bromide; MW: Molecular weight; MWCO: Molecular weight cut-off; N2B: Nose-to-brain; NFT: Neurofibrillary tangle; NLC: Nanostructured lipid carrier; PBS: Phosphate-buffered saline; PDI: Polydispersity index; QbD: Quality by Design; RMS: Root mean square; RSM: Response surface methodology; SD: Standard deviation; SLN:

Solid lipid nanoparticle; SNF: Simulated nasal fluid; STPP: Sodium tripolyphosphate; XRD: X-ray diffraction.

REFERENCES

1. World Health Organization. Global status report on the public health response to dementia. Geneva: WHO; 2021.
2. Nichols E, Steinmetz JD, Vollset SE, et al. Estimation of the global prevalence of dementia in 2019 and forecasted prevalence in 2050: an analysis for the Global Burden of Disease Study 2019. Lancet Public Health. 2022;7(2):e105–e125.
3. Hardy J, Selkoe DJ. The amyloid hypothesis of Alzheimer's disease: progress and problems on the road to therapeutics. Science. 2002;297(5580):353–356.
4. Ferreira-Vieira TH, Guimaraes IM, Silva FR, Ribeiro FM. Alzheimer's disease: targeting the cholinergic system. Curr Neuropharmacol. 2016;14(1):101–115.
5. Birks JS, Harvey RJ. Donepezil for dementia due to Alzheimer's disease. Cochrane Database Syst Rev. 2018;6(6):CD001190.
6. Sugimoto H. Donepezil hydrochloride: a treatment drug for Alzheimer's disease. Chem Rec. 2001;1(1):63–73.
7. Bhowmik A, Khan R, Ghosh MK. Blood-brain barrier: a challenge for effectual therapy of brain tumors. Biomed Res Int. 2015;2015:320941.
8. Pardridge WM. The blood-brain barrier: bottleneck in brain drug development. NeuroRx. 2005;2(1):3–14.
9. Masserini M. Nanoparticles for brain drug delivery. ISRN Biochem. 2013;2013:238428.
10. Pires PC, Rodrigues M, Alves G, Santos AO. Strategies to improve drug strength in nasal preparations for brain delivery of low aqueous solubility drugs. Pharmaceutics. 2022;14(3):588.
11. Dhuria SV, Hanson LR, Frey WH 2nd. Intranasal delivery to the central nervous system: mechanisms and experimental considerations. J Pharm Sci. 2010;99(4):1654–1673.
12. Thorne RG, Bhowmick S, Bhowmick A. Intranasal drug delivery to the brain: advances and future perspectives. Drug Discov Today. 2023;28(7):103600.
13. Grassin-Delyle S, Buenestado A, Naline E, et al. Intranasal drug delivery: an efficient and non-invasive route for systemic administration. Pharmacol Ther. 2012;134(3):366–379.
14. Cunha S, Swedrowska M, Bellahnid Y, et al. Thermosensitive in situ hydrogels of rivastigmine-loaded lipid-based nanosystems for nose-to-brain delivery: characterization, biocompatibility, and drug deposition studies. Int J Pharm. 2022;616:121557.
15. Muchow M, Maincent P, Müller RH. Lipid nanoparticles with a solid matrix (SLN, NLC, LDC) for oral drug delivery. Drug Dev Ind Pharm. 2008;34(12):1394–1405.
16. Ezzati Nazhad Dolatabadi J, Valizadeh H, Hamishehkar H. Solid lipid nanoparticles as efficient drug and gene delivery systems: recent breakthroughs. Adv Pharm Bull. 2015;5(2):151–159.
17. Mazzarino L, Travelet C, Ortega-Murillo S, et al. Elaboration of chitosan-coated nanoparticles loaded with curcumin for mucoadhesive applications. J Colloid Interface Sci. 2012;370(1):58–66.
18. Bernkop-Schnürch A, Dünnhaupt S. Chitosan-based drug delivery systems. Eur J Pharm Biopharm. 2012;81(3):463–469.
19. Patel S, Chavhan S, Soni H, et al. Brain targeting of sumatriptan succinate using chitosan nanoparticles: intranasal versus intravenous route. J Pharm Pharmacol. 2011;63(9):1169–1175.
20. Md S, Haque S, Madheswaran T, et al. Brain targeted intranasal delivery of lamotrigine-loaded mucoadhesive nanoemulsion for the treatment of epilepsy. Drug Dev Ind Pharm. 2021;47(1):1–11.
21. ICH Harmonised Tripartite Guideline: Pharmaceutical Development Q8(R2). International Conference on Harmonisation; 2009.
22. Ferreira SLC, Bruns RE, Ferreira HS, et al. Box-Behnken design: an alternative for the optimization of analytical methods. Anal Chim Acta. 2007;597(2):179–186.
23. Alam MI, Baboota S, Ahuja A, et al. Intranasal administration of nanostructured lipid carriers containing CNS acting drug: pharmacodynamic studies and estimation in blood and brain. J Psychiatr Res. 2012;46(9):1133–1138.
24. Elnaggar YS, El-Massik MA, Abdallah OY. Self-nanoemulsifying drug delivery systems of tamoxifen citrate: design and optimization. Int J Pharm. 2009;380(1–2):133–141.
25. Kaur P, Garg T, Rath G, Goyal AK. In situ nasal gel drug delivery: a novel approach for brain targeting through the intranasal route. Artif Cells Nanomed Biotechnol. 2016;44(4):1167–1176.
26. Madgulkar A, Bhalekar M, Padalkar R. In vitro studies on mucoadhesive and permeation enhancement properties of N-trimethyl chitosan (TMC) modified microspheres for nasal drug delivery. Curr Drug Deliv. 2009;6(3):215–221.
27. Ugwoke MI, Agu RU, Verbeke N, Kinget R. Nasal mucoadhesive drug delivery: background, applications, trends and future perspectives. Adv Drug Deliv Rev. 2005;57(11):1640–1665.
28. Mosmann T. Rapid colorimetric assay for cellular growth and survival: application to proliferation and cytotoxicity assays. J Immunol Methods. 1983;65(1–2):55–63.
29. Berman HM, Westbrook J, Feng Z, et al. The Protein Data Bank. Nucleic Acids Res. 2000;28(1):235–242.
30. Vyas TK, Babbar AK, Sharma RK, Singh S, Misra A. Preliminary brain-targeting studies on intranasal

mucoadhesive microemulsions of sumatriptan. AAPS PharmSciTech. 2006;7(1):E49–E57.
31. Ganesan P, Narayanasamy D. Lipid nanoparticles: different preparation techniques, characterization, hurdles, and strategies for the production of solid lipid nanoparticles and nanostructured lipid carriers for oral drug delivery. Sustain Chem Pharm. 2017;6:37–56.
32. Jaiswal M, Dudhe R, Sharma PK. Nanoemulsion: an advanced mode of drug delivery system. 3 Biotech. 2015;5(2):123–127.
33. Rao JP, Geckeler KE. Polymer nanoparticles: preparation techniques and size-control parameters. Prog Polym Sci. 2011;36(7):887–913.
34. Sogias IA, Williams AC, Khutoryanskiy VV. Why is chitosan mucoadhesive? Biomacromolecules. 2008;9(7):1837–1842.
35. Mistry A, Stolnik S, Illum L. Nanoparticles for direct nose-to-brain delivery of drugs. Int J Pharm. 2009;379(1):146–157.
36. Costa P, Sousa Lobo JM. Modeling and comparison of dissolution profiles. Eur J Pharm Sci. 2001;13(2):123–133.
37. Negi JS, Singh S, Joshi GP, Rawat MS, Galber BN. Central nervous system stimulating effect of chitosan-based nanoparticles of donepezil: pharmacodynamic and pharmacokinetic studies on aged rats. Drug Dev Ind Pharm. 2013;39(9):1404–1410.
38. Bhatt R, Bhattamisra SK, Bhatt DK, Ramani YR. Donepezil-loaded nanostructured lipid carriers for brain targeting via nasal route. Pharm Nanotechnol. 2023;11(2):134–148.
39. Bhavna B, Ali M, Ali R, et al. Donepezil-loaded chitosan nanoparticles for nasal delivery to the brain: in vitro characterization and in vivo anti-dementia evaluation. J Biomater Appl. 2014;29(2):284–296.
40. Czajkowska-Kosnik A, Szekalska M, Winnicka K. Nanostructured lipid carriers for drug delivery. Drug Discov Today Technol. 2019;34:1–8.